Zitierweise: *Angew. Chem. Int. Ed.* **2022,** *61,* e202117455
Internationale Ausgabe: doi.org/10.1002/anie.202117455
Deutsche Ausgabe: doi.org/10.1002/ange.202117455

Metal–Organic Frameworks

Coloration in Supraparticles Assembled from Polyhedral Metal-Organic Framework Particles

Junwei Wang[+], Yang Liu[+], Gudrun Bleyer, Eric S. A. Goerlitzer, Silvan Englisch, Thomas Przybilla, Chrameh Fru Mbah, Michael Engel, Erdmann Spiecker, Inhar Imaz, Daniel Maspoch,* and Nicolas Vogel**

Abstract: Supraparticles are spherical colloidal crystals prepared by confined self-assembly processes. A particularly appealing property of these microscale structures is the structural color arising from interference of light with their building blocks. Here, we assemble supraparticles with high structural order that exhibit coloration from uniform, polyhedral metal–organic framework (MOF) particles. We analyse the structural coloration as a function of the size of these anisotropic building blocks and their internal structure. We attribute the angle-dependent coloration of the MOF supraparticles to the presence of ordered, onion-like layers at the outermost regions. Surprisingly, even though different shapes of the MOF particles have different propensities to form these onion layers, all supraparticle dispersions show well-visible macroscopic coloration, indicating that local ordering is sufficient to generate interference effects.

[*] Dr. J. Wang,[+] G. Bleyer, Dr. E. S. A. Goerlitzer, Prof. Dr. N. Vogel
Institute of Particle Technology, Friedrich-Alexander Universität Erlangen-Nürnberg, 91058 Erlangen (Germany)
E-mail: nicolas.vogel@fau.de

Y. Liu,[+] Dr. I. Imaz, Prof. Dr. D. Maspoch
Catalan Institute of Nanoscience and Nanotechnology (ICN2), CSIC & The Barcelona Institute of Science and Technology, Bellaterra, 08193 Barcelona (Spain)
E-mail: inhar.imaz@icn2.cat
daniel.maspoch@icn2.cat

S. Englisch, Dr. T. Przybilla, Prof. Dr. E. Spiecker
Institute of Micro- and Nanostructure Research (IMN), Center for Nanoanalysis and Electron Microscopy (CENEM), IZNF, Friedrich-Alexander Universität Erlangen-Nürnberg, 91058 Erlangen (Germany)

Dr. C. F. Mbah, Prof. Dr. M. Engel
Institute for Multiscale Simulation, IZNF, Friedrich-Alexander Universität Erlangen-Nürnberg, 91058 Erlangen (Germany)

Prof. Dr. D. Maspoch
ICREA, Pg. Lluis Companys 23, 08010 Barcelona (Spain)

[+] These authors contributed equally to this work.

© 2022 The Authors. Angewandte Chemie published by Wiley-VCH GmbH. This is an open access article under the terms of the Creative Commons Attribution Non-Commercial NoDerivs License, which permits use and distribution in any medium, provided the original work is properly cited, the use is non-commercial and no modifications or adaptations are made.

Introduction

Emerging functional materials for applications in photonics, plasmonics, and mechanics are created by assembling smaller particles into defined structures.[1] Among various assembly strategies, using spherical confinements (e.g. in drying emulsion droplets) to guide the self-assembly process is garnering increasing interest.[2] This hierarchical approach entails assembly of a finite number of particles into a larger supraparticle. The finite number can provide additional effects, such as fluctuations of the thermodynamic stability of defined clusters.[2g] More generally, ordered supraparticles exhibit the collective properties present in their corresponding bulk assemblies, while remaining dispersible, discrete objects that are easy to handle and post-process. For supraparticles whose constituent particles are of a size in the range of visible light wavelengths, the regular internal structure causes light diffraction, with constructive and destructive interference occurring for specific ranges of wavelengths that depend on the particle size, lattice spacing, degree of order, and materials composition (namely the variations in the refractive index), all of which affect the resulting structural color and its angle dependence, thus generating structural color. The hue, intensity and saturation of this color depends on the refractive index, degree of crystallinity and crystal-type of the supraparticle.[3,4a]

To date, most supraparticles exhibiting structural color are assembled from spherical primary particles. Significant efforts have been focused on varying the type of the primary spherical particles, including polystyrene, silica and melanin and other biopolymers.[1c,4] The extensive use of spherical primary particles in supraparticles stems from their availability and strong tendency to form close-packed, ordered structures. At the same time, the type of resulting crystal lattices is often limited to close-packings of equal spheres. In contrast, the variety of ordered structures that can be formed by polyhedral particles with potential distinct optical functionalities is massive.[5] Although researchers can now exercise precise control over the size and shape of diverse polyhedral particles (mainly metallic ones), they continue to face the challenge of assembling these particles within droplets to generate supraparticles with structural color. This is because the particles are either too small to produce Bragg diffraction color or too heavy to remain dispersed within the droplets, so that sedimenta-

© 2022 The Authors. Angewandte Chemie published by Wiley-VCH GmbH

15213757, 2022, 16, Downloaded from https://onlinelibrary.wiley.com/doi/10.1002/ange.202117455 by Readcube (Labtiva Inc.), Wiley Online Library on [27/10/2022]. See the Terms and Conditions (https://onlinelibrary.wiley.com/terms-and-conditions) on Wiley Online Library for rules of use; OA articles are governed by the applicable Creative Commons License

tion impedes efficient equilibration.[6] This, in turn, precludes the use of many functional materials that are intrinsically polyhedral in the assembly of new multifunctional supraparticles.

To face this challenge, we envisaged using polyhedral metal–organic frameworks (MOFs) as primary particles for the formation of supraparticles. MOFs are functional porous materials with large surface areas and potential for myriad applications such as gas storage, catalysis and separation.[7] MOFs also exist in the form of crystalline particles that encompass most known polyhedral shapes. Moreover, they have been recently synthesized with highly homogeneous, tunable size and shape.[8] Together with their low density and their amenability to surface functionalization, MOFs can also be obtained as stable colloids, with particle sizes in the range of ≈200 nm to 400 nm, which is in the ideal range to interact with visible light and thus, produce structural color. Indeed, we have recently demonstrated the use of such polyhedral MOF particles for three-dimensional photonic MOF superstructures.[9,10] Here, we demonstrate that similar complex-shaped MOF particles can self-assemble within the confinement of an emulsion droplet and form spherical, consolidated and ordered photonic supraparticles. In the following, we examine in detail how the spherical confinement affects the resultant self-assembled structure and how this internal structure translates into macroscopically observable structural color.

The polyhedral MOF particles used in this study are cubic zeolitic imidazolate framework-8 (C-ZIF-8), truncated rhombic dodecahedral TRD-ZIF-8, perfect rhombic dodecahedral RD-ZIF-8 and octahedral Universitetet i Oslo-66 (O-UiO-66) particles. ZIF-8 is a porous MOF made of Zn^{II} ions and 2-methylimidazolate (2-Mim) linkers that exhibits a sodalite-type structure and a large surface area (≈1200–1500 $m^2 g^{-1}$).[11] UiO-66 is a MOF built up from bridging $[Zr_6O_4(OH)_4]$ clusters by terephthalic acid linkers, also showing a large surface area (≈1200 $m^2 g^{-1}$).[12] We found that the spherical geometry of each supraparticle enforces ordered, onion-like layered structures of polyhedral MOF particles, which, in turn, act as Bragg reflectors and cause interference effects leading to structural coloration. Based on our results, we discuss the angle-dependent coloration as a function of the size and shape of the building blocks and the internal order of the resultant supraparticles.

Results and Discussion

We began with the synthesis of different colloidal polyhedral MOF particles (Figure 1a; Figure S1–S4). C-ZIF-8 particles were synthesized by reacting an aqueous mixture of $Zn(NO_3)_2{\cdot}6H_2O$, 2-Mim and cetyltrimethylammonium bromide (CTAB) at room temperature for 5 h. Similarly, both TRD- and RD-ZIF-8 particles were prepared by reacting an aqueous solution of $ZnAc_2{\cdot}2H_2O$, 2-Mim and CTAB (only in the case of TRD-ZIF-8) at room temperature for 2 h. In the case of O-UiO-66, a dimethylformamide (DMF) solution of $ZrCl_4$, terephthalic acid and acetic acid was heated at 120 °C for 12 h. Afterwards, the three types of ZIF-8 particles were washed with deionized water and O-UiO-66 with DMF by centrifugation at 9000 rpm in 50 mL Falcon tubes. Colloids were finally prepared at concentrations of 40 mg mL^{-1} (C-ZIF-8), 40 mg mL^{-1} (TRD-ZIF-8), 20 mg mL^{-1} (RD-ZIF-8) and 6 mg mL^{-1} (O-UiO-66). Field-emission scanning electron microscopy (FESEM), powder X-ray diffraction (PXRD), and zeta-potential measurements of the resulting colloids revealed the formation of the following homogeneous particles, listed here with their respective particle sizes: C-ZIF-8 (191 ± 9 nm; Figure S1), TRD-ZIF-8 (181 ± 9 nm; 198 ± 10 nm; 229 ± 9 nm; and 247 ± 10 nm; Figure S2), RD-ZIF-8 (246 ± 12 nm; 267 ± 12 nm; and 293 ± 13 nm; Figure S3) and O-UiO-66 (edge size: 194 ± 12 nm; 238 ± 13 nm; and 247 ± 13 nm; Figure S4). The truncation in TRD-ZIF-8 particles was 0.68. The surface charge of all the ZIF-8 particles was approximately +30 mV, for the O-UiO-66 particles, ca. +45 mV.

Having prepared the four types of MOF particles, we then synthesized the corresponding supraparticles. This began with addition of 0.5 wt% non-ionic alcohol ethoxylate surfactant (Lutensol TO-8, BASF) into separate 1.0 mL dispersions of the ZIF-8 particles, and of polyvinylpyrrolidone into a dispersion of the UiO-66 particles to improve colloidal stability. Three centrifugation cycles removed residual reagents, including excess surfactant. Next, the aqueous MOF particle dispersions were emulsified in perfluorinated oil (HFE 7500), either by vigorous shaking (Figure S5) or by droplet-based microfluidics (Figure 1b,c, Figure S6). The droplets were stabilized by a perflurosurfactant and left in an open glass vial overnight to allow evaporation and self-organization of the building blocks inside the droplets.

Next, we characterized the supraparticles assembled from each of the four polyhedral MOF particles by FESEM (Figures 1d). Each supraparticle was spherical and had an ordered surface, in which each class of polyhedral MOF particle was packed in agreement with the corresponding Monte Carlo simulations of hard polyhedra in spherical confinement (Figures 1e). The RD- and TRD-ZIF-8 particles formed a triangular unit cell and a rhombic unit cell at the supraparticle surface, respectively, agreeing with their bulk face-centered cubic packing and rhombohedral packing.[9] The C-ZIF-8 particles formed the expected square unit cell on the spherical supraparticle surface, whereas the O-UiO-66 particles formed a triangular cell. Careful analysis of FESEM images also showed that the flat faces of the TRD-ZIF-8, C-ZIF-8 and O-UiO-66 particles were exposed to form a smooth, ordered, supraparticle surface. This was observed both experimentally and in the simulations. We reason that this packing is caused by entropic force that favors face-to-face configurations and disfavors vertex-to-face configurations in polyhedral packing, which tends to align the flat faces of particles to the droplet interface.[13]

Spherical confinement distorts crystalline lattices; consequently, it distorts the arrangement of MOF particles inside the supraparticles.[2f,g,14,15] The spherical curvature forces the primary particle to form a spherical particle monolayer at the supraparticle surface, which can in turn

© 2022 The Authors. Angewandte Chemie published by Wiley-VCH GmbH

15213757, 2022, 16, Downloaded from https://onlinelibrary.wiley.com/doi/10.1002/ange.202117455 by Readcube (Labtiva Inc.), Wiley Online Library on [27/10/2022]. See the Terms and Conditions (https://onlinelibrary.wiley.com/terms-and-conditions) on Wiley Online Library for rules of use; OA articles are governed by the applicable Creative Commons License

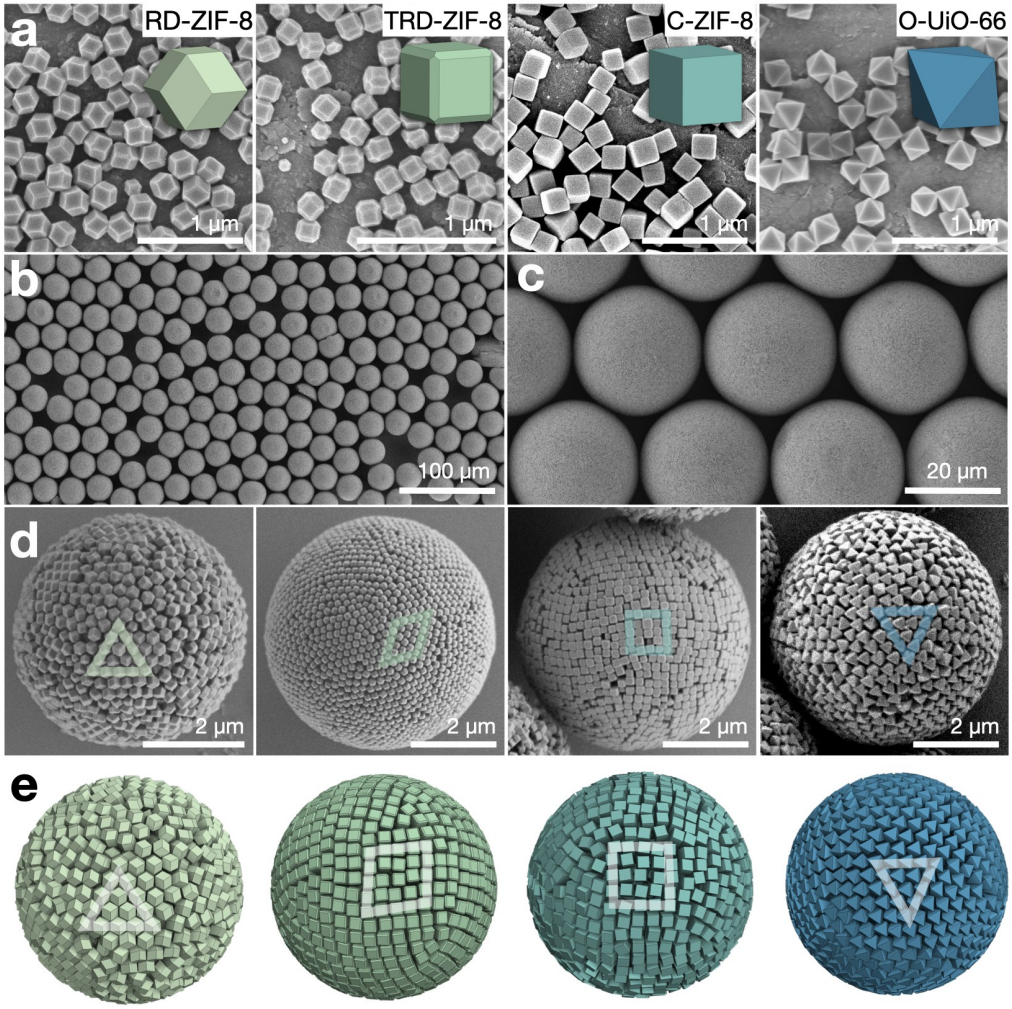

Figure 1. Supraparticles from uniform, polyhedral MOF building blocks. a) FESEM of monodisperse rhombic dodecahedron (RD-ZIF-8), truncated rhombic dodecahedron (TRD-ZIF-8), cube (C-ZIF-8) and octahedron (O-UiO-66) particles (left to right). b, c) Monodisperse TRD-ZIF-8 supraparticles prepared by emulsifying the MOF particle dispersion using droplet-based microfluidics. d) FESEM (from left to right) of RD-ZIF-8, TRD-ZIF-8, C-ZIF-8 and O-UiO-66 supraparticles, exhibiting ordered surfaces and characteristic packings. e) Snapshots of Monte Carlo simulations with polyhedra in spherical confinement.

cause the particles underneath to form another ordered layer. This curvature effect propagates from the surface of the supraparticle towards the interior and attenuates as the curvature increases up to infinity at the core. This suggests that the supraparticle might exhibit onion-like concentric layer structures under the surface,[2c] and that the thickness of these onion layers may differ depending on the propensity of the differently-shaped particles to assemble in the spherical confinement.

We confirmed this hypothesis by two independent imaging techniques, namely X-ray tomography and focused ion beam (FIB)-assisted cross-sectioning, providing direct insight into the inner structure of the different supraparticles (Figure 2). Figure 2a shows an X-ray transmission image of a supraparticle assembled from C-ZIF-8 particles, where up to ten concentric layers, forming an ordered, onion-like structure, are evident near the surface. Towards the center, the image appears homogeneous, indicating the particles are less ordered at the core of the supraparticle. Similarly, pronounced onion-like layer structures were observed in TRD-ZIF-8 supraparticles, while RD-ZIF-8 and O-UiO-66 supraparticles showed only little onion layers (Figure S7). The impression of the X-ray tomography was corroborated by SEM-FIB cross sectioning (Figure 2b–e). Onion-like layers were observed for all ZIF-8 polyhedral MOF particles near the supraparticle surface, conforming to the spherical curvature. Corroborating the X-ray images, the RD-ZIF-8 and the O-UiO-66 supraparticles only showed lower propensities to form onion-like layers and mostly regions with short-range order (Figure 2b, e; Figure S8, S11), whereas TRD- and C-ZIF-8 supraparticles exhibited pronounced onion-like layers penetrating far towards the interior (Figure 2c, d; Figure S9, S10). Intriguingly, the TRD-ZIF-8 supraparticles exhibited very high crystallinity throughout

© 2022 The Authors. Angewandte Chemie published by Wiley-VCH GmbH

15213757, 2022, 16, Downloaded from https://onlinelibrary.wiley.com/doi/10.1002/ange.202117455 by Readcube (Labtiva Inc.), Wiley Online Library on [27/10/2022]. See the Terms and Conditions (https://onlinelibrary.wiley.com/terms-and-conditions) on Wiley Online Library for rules of use; OA articles are governed by the applicable Creative Commons License

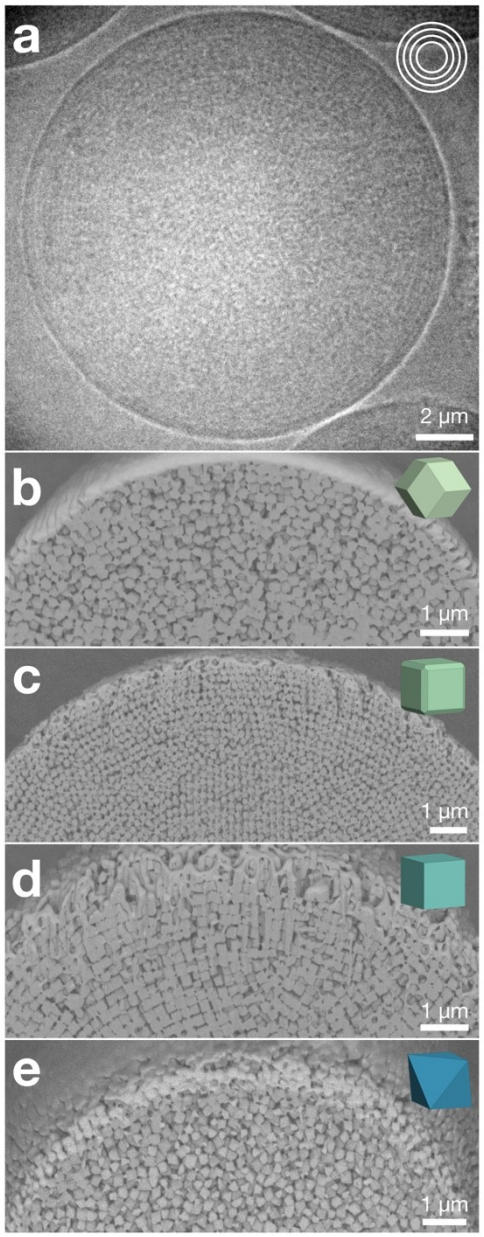

Figure 2. Internal structure of the supraparticles assembled from polyhedral MOFs. a) X-ray transmission image of a C-ZIF-8 supraparticle, showing its onion-like structure near the outer surface. b)–e) Focused ion beam cross-sections of a RD-ZIF-8 (b), TRD-ZIF-8 (c), C-ZIF-8 (d) and O-UiO-66 (e) supraparticles, showing their corresponding thicknesses of the onion-like layers.

the interior, albeit in multiple crystalline domains. We reason that sufficient equilibration may enable them to evolve towards complete crystallization with global symmetry, similar to what has been observed in spherical particles or ultra-small nanocrystals in spherical confinement.[2f,g,6a] Indeed, we occasionally found local five-fold patterns in small supraparticles of TRD-ZIF-8 particles, indicative of an emerging icosahedral symmetry, corroborating results on the equilibrium structure of cubic nanoparticles with truncated edges (Figure S12).[6a] Interestingly, in the Monte-Carlo simulations, all four hard polyhedral particles form onion-like layers of similar thickness, indicating that shape itself does not cause the different propensity to form onion-like layers in differently-shaped MOF particles (Figure 1e, Figure S13). However, in a simple bulk crystallization induced by centrifugation, we observed coloration for the TRD- and C-ZIF-8 particles, but not for the RD-ZIF-8 and O-UiO-66 particles (Figure S14), agreeing with the observed trend in the supraparticles. We therefore hypothesize that the effect may be caused by the anisotropic electrostatic repulsions of polyhedral particles. It is likely that there is more screening of charges at sharp edges, i.e. the RD-ZIF-8 particles, making them more prone to aggregate at close distance, compared to C-ZIF-8 with less edges. TRD-ZIF-8 particles on the other hand have rounded and smoothened edges, making such particles even more stable.[16]

The ability to form well-ordered MOF supraparticles with defined internal structure enabled us to study their photonic properties as a function of primary particle shape and degree of internal order (Figure 3). To this end, we combined micro-spectroscopy at the individual supraparticle level on a substrate in air with macroscopic angle-dependent spectroscopy of the supraparticle dispersions. First, we assembled four types of supraparticles and chose the primary particle sizes that produce a green reflection color under the microscope (Figure 3, top). As expected from the investigation of internal order (Figure 2), C-ZIF-8 and TRD-ZIF-8 supraparticles showed a pronounced green coloration with a well-resolved central colored dot, which results from constructive interference of light reflected at the spherical-symmetric ordered onion layers (Figure 3b,c). In contrast, RD-ZIF-8 and O-UiO-66 supraparticles showed a less pronounced reflection color (Figure 3a,d), indicative of the lower degree of internal ordering. Noteworthily, the surfaces of all supraparticles exhibited well-ordered arrangements of particles (Figure 3a–d, middle), indicating that polydispersity is not the origin of the reduced order of some shapes. Microscopic reflection spectra (Figure 3a–d, bottom) corroborated these observations. TRD- and C-ZIF-8 supraparticles showed narrower and more defined photonic stop bands (full width at half maximum (FWHM) = 66 nm and 56 nm, respectively), while RD-ZIF-8 and O-UiO-66 supraparticles exhibited broader peaks (FWHM = 84 nm and 83 nm, respectively).

Next, we used the TRD-ZIF-8 (229 nm) sample to exemplarily establish the relationship between supraparticle size and the reflection color intensity, measured at the peak of the photonic stop band (Figure 3e), using a polydisperse supraparticle sample prepared by simple shaking emulsification. A clear increase in color intensity was observed with increasing supraparticle size, which can be rationalized from the diminishing effect of frustrated crystallization caused by the curvature of the spherical confinement.

We then established the relationship between primary particle dimensions and the structural color of the supraparticles. We systematically varied the sizes of the differently-shaped MOF particles and measured reflection spectra from the formed MOF supraparticles suspended in the oil phase in a glass vial (Figure 3f). The reflection peaks of all

© 2022 The Authors. Angewandte Chemie published by Wiley-VCH GmbH

15213757, 2022, 16, Downloaded from https://onlinelibrary.wiley.com/doi/10.1002/ange.202117455 by Readcube (Labtiva Inc.), Wiley Online Library on [27/10/2022]. See the Terms and Conditions (https://onlinelibrary.wiley.com/terms-and-conditions) on Wiley Online Library for rules of use; OA articles are governed by the applicable Creative Commons License

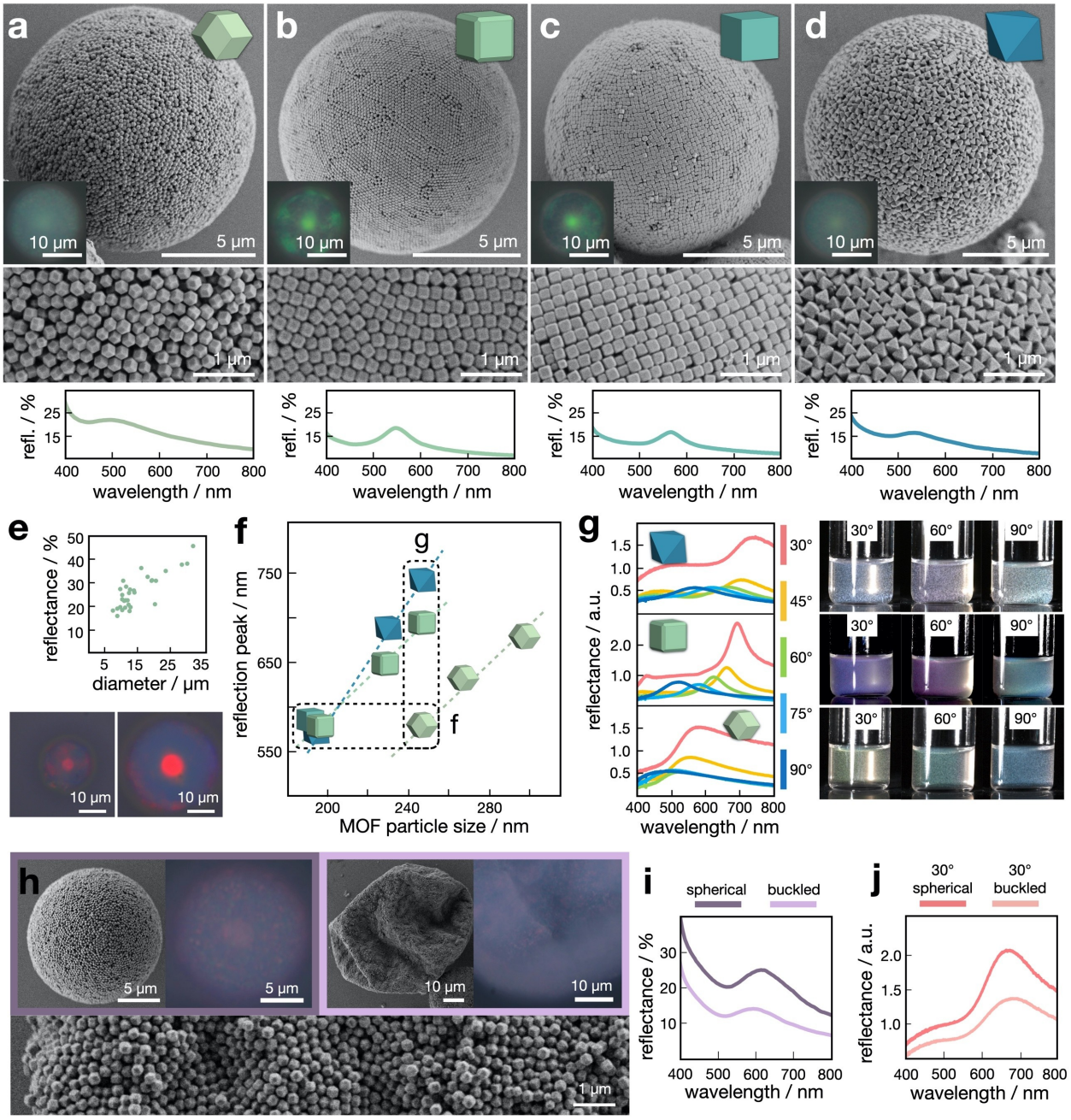

Figure 3. Optical properties of MOF supraparticles. a)–d) Top row: FESEM of RD-ZIF-8 (a), TRD-ZIF-8 (b), C-ZIF-8 (c) and O-UiO-66 (d) supraparticles, exhibiting structural coloration from the interaction of the incident light and the supraparticle structure (optical microscopy images in inset). Middle row: magnification of the particle surfaces, showing well-ordered arrangements of the primary particles; bottom row: reflection spectra measured for individual supraparticles. e) Effect of supraparticle size on the intensity of the photonic stop band, exemplarily shown for TRD-ZIF-8 supraparticles. f) Relationship between size and shape of the primary particles on the wavelength of the reflection peak, measured in suspension. g) Angle-dependent reflectance spectra of MOF supraparticles consisting of the same colloidal particle size but different shapes, along with corresponding photographs showing the observable coloration. h) FESEM of spherical and buckled MOF supraparticles, with optical microscopy images showing differences in structural color. The surface of the buckled supraparticle shows the hexagonally-packed particle layer. i) Reflectance spectra of individual spherical and buckled MOF supraparticles. j) Reflectance spectra of spherical and buckled supraparticles measured in suspension.

samples shifted linearly with increasing primary particle size, as the periodicity in the Bragg diffractor scales linearly with the particle size. Noteworthily, larger RD-ZIF-8 particles are required to produce the same reflection peak compared to other shapes (horizontal box in Figure 3f). As shown in Figure 3a–d, a green reflection color was produced for TRD-ZIF-8 (197 nm), C-ZIF-8 (191 nm) and O-UiO-66 (194 nm) of similar sizes, while RD-ZIF-8 had significantly larger dimensions (246 nm). These differences are caused by the packing of the differently-shaped particles. Entropy

© 2022 The Authors. Angewandte Chemie published by Wiley-VCH GmbH

15213757, 2022, 16, Downloaded from https://onlinelibrary.wiley.com/doi/10.1002/ange.202117455 by Readcube (Labtiva Inc.), Wiley Online Library on [27/10/2022]. See the Terms and Conditions (https://onlinelibrary.wiley.com/terms-and-conditions) on Wiley Online Library for rules of use; OA articles are governed by the applicable Creative Commons License

favors the particles to align their faces within each layer and between layers (Figure S15).[17] For TRD- (and similar for C-shaped) particles, the surface of a close-packed layer is "flat", leaving only small grooves from the truncation at particle edges. As a result, the distance between two stacked layers is the same as the distance between the two opposite faces of the TRD, which is the particle size by definition (note that this does not equal the edge length, Figure S2). However, for RD-ZIF-8 particles, the surface of a close-packed layer has jagged protrusions and indentations (Figure S15). When two such layers stack, protrusions and indentations can register, bringing the two layers closer. As a result, the distance between layers is smaller than the size of RD-shaped particles. From Figure 3f, we estimate that RD-shaped particles need to be 1.25 larger in size (than TRD-shaped particles) to produce a similar Bragg reflection peak.

We then focused on the macroscopic, angle-dependent coloration of the different MOF supraparticles, which was measured directly in suspension using a collimated white light source at different angles for illumination (Figure S16). Figure 3g shows the spectra of supraparticle suspension prepared by shaking using similar-sized primary particles of different shapes ($\approx$247 nm; vertical box in Figure 3f). As established above, the different packings of the individual shapes lead to different layer spacing and therefore a different photonic stop band at the same illumination angle (Figure 3f). Note that the reduced refractive index contrast in suspension efficiently suppress incoherent scattering, manifested by reduced reflection at lower wavelengths around 400 nm compared to samples measured in air (Figure 3a–d). As the angle between incident light and detector increases from 30° to 90°, all supraparticle suspensions showed a blue shift of the photonic stop band (Figure 3g, Figure S17). A quantitative comparison between all samples revealed nearly identical angle-dependent blue shifts of the stop band, regardless of the primary particle shape (Figure S18), suggesting that interference of light reflected at the onion-like layers is the dominating color mechanism. However, it is noteworthy that the RD-ZIF-8 and O-UiO-66 supraparticles with low propensity to form onion layers and thus low reflected color intensity under the microscope (Figure 3a, d), also showed evident macroscopic coloration. We note that the spectral intensities of the different samples cannot be directly compared, as the mobile supraparticles rapidly accumulate on the top of the suspension due to the density difference, causing a non-uniform concentration during measurements. Nevertheless, the macroscopic photographs (Figure 3g) of the different dispersions document the visible, angle-dependent coloration of the RD-ZIF-8 and O-UiO-66 supraparticle dispersions with comparably low order.

Interestingly, even buckled MOF supraparticles with supposedly compromised internal order exhibited observable structural color (Figure 3h). We fabricated spherical and buckled RD-ZIF-8 supraparticles by systematically removing surfactant via additional centrifugation steps (Figure S19). The buckled supraparticles did not show the typical central dot attributed to the onion-like layers in the optical microscopy images (Figure 3h).[3a] Their spectral properties, however, showed the presence of a reflection peak (Figure 3i,j). A similar phenomenon was recently reported for nanocellulose crystals in droplets, where multilayer structures persist through a buckled morphology.[18] It is possible that the MOF particles also form stacked, non-concentric layers near the supraparticles surface. However, due to the larger and more rigid particle nature, only a few layers can be reasonably expected under the heavily buckled surface. Additionally, the reported buckled nanocellulose structures exhibit angle-independent color, while the buckled MOF supraparticles maintain the same angle-dependency observed in spherical supraparticles (Figure S20). We hypothesize that other mechanisms may contribute to this coloration. One possibility is an additional surface grating effect (Figure S21).[19–21] We noticed that even for buckled supraparticles, the surface consists of hexagonally close-packed particles with sufficient structural order (Figure 3h, inset, Figure S22), similar to the surface of spherical supraparticles (Figure S23). The inclined angle enabled by the polyhedral particles may efficiently diffract part of the incident light, which adds to the weaker Bragg reflection color for the buckled supraparticles. Another possible source for the color is the existence of numerous tiny crystallites consisting of a few dozen particles randomly distributed in the supraparticles, which can be seen in the weak and localized color patches in the optical microscopic image (Figure 3h). While the exact mechanism and the individual contributions to the observed structural color of MOF supraparticles requires more detailed studies supported by numerical simulations, the existence of macroscopic coloration in less ordered structure with non-spherical, buckled morphology is promising for the design of structurally colored materials and pigments.

Conclusion

In conclusion, we assembled various type of polyhedral MOF particles into well-defined MOF supraparticles and investigated the shape-dependent internal structure. We then correlated this internal order with microscopic and macroscopic structural coloration and established shape-size-coloration relationships. With the growing library of MOF particle materials and shapes, our study opens a new avenue to fabricate discrete hierarchical ordered structures that combine intrinsic MOF functionality with additional emerging collective properties.

Acknowledgements

We thank C.X. Du and E.G. Teich for discussion of polyhedra packing in confinement. This work was supported by the Spanish MINECO (project RTI2018-095622-B-I00) and the Catalan AGAUR (project 2017 SGR 238). It was also funded by the CERCA Pro-gram/Generalitat de Catalunya. ICN2 is supported by the Severo Ochoa program from the Spanish MINECO (Grant No. SEV-2017-0706).

© 2022 The Authors. Angewandte Chemie published by Wiley-VCH GmbH

15213757, 2022, 16, Downloaded from https://onlinelibrary.wiley.com/doi/10.1002/ange.202117455 by Readcube (Labtiva Inc.), Wiley Online Library on [27/10/2022]. See the Terms and Conditions (https://onlinelibrary.wiley.com/terms-and-conditions) on Wiley Online Library for rules of use; OA articles are governed by the applicable Creative Commons License

Y.L. acknowledges the China Scholarship Council for scholarship support. T.P. and S.E. acknowledges support by DFG within the framework of the research training group GRK 1896. This research was supported by the Deutsche Forschungsgemeinschaft (DFG, German Research Foundation)—Project-ID 416229255—SFB 1411. N.V. and M.E. also acknowledge funding by the DFG under projects VO 1824/7-1 and EN 905/2-1, respectively. Open Access funding enabled and organized by Projekt DEAL.

Conflict of Interest

The authors declare no conflict of interest.

Data Availability Statement

The data that support the findings of this study are available from the corresponding author upon reasonable request.

Keywords: Emulsion · Metal–Organic Frameworks · Self-Assembly · Structural Color · Supraparticles

[1] a) J. F. Galisteo-López, M. Ibisate, R. Sapienza, L. S. Froufe-Pérez, Á. Blanco, C. López, *Adv. Mater.* **2011**, *23*, 30; b) M. He, J. P. Gales, É. Ducrot, Z. Gong, G.-R. Yi, S. Sacanna, D. J. Pine, *Nature* **2020**, *585*, 524–529; c) A. Dreyer, A. Feld, A. Kornowski, E. D. Yilmaz, H. Noei, A. Meyer, T. Krekeler, C. Jiao, A. Stierle, V. Abetz, H. Weller, G. A. Schneider, *Nat. Mater.* **2016**, *15*, 522; d) N. S. Mueller, Y. Okamura, B. G. M. Vieira, S. Juergensen, H. Lange, E. B. Barros, F. Schulz, S. Reich, *Nature* **2020**, *583*, 780.

[2] a) M. A. Boles, M. Engel, D. V. Talapin, *Chem. Rev.* **2016**, *116*, 11220; b) N. Vogel, M. Retsch, C. A. Fustin, A. Del Campo, U. Jonas, *Chem. Rev.* **2015**, *115*, 6265; c) R. M. Parker, B. Frka-Petesic, G. Guidetti, G. Kamita, G. Consani, C. Abell, S. Vignolini, *ACS Nano* **2016**, *10*, 8443; d) T. Wang, D. LaMontagne, J. Lynch, J. Q. Zhuang, Y. C. Cao, *Chem. Soc. Rev.* **2013**, *42*, 2804; e) S. Wintzheimer, T. Granath, M. Oppmann, T. Kister, T. Thai, T. Kraus, N. Vogel, K. Mandel, *ACS Nano* **2018**, *12*, 5093; f) B. de Nijs, S. Dussi, F. Smallenburg, J. D. Meeldijk, D. J. Groenendijk, L. Filion, A. Imhof, A. van Blaaderen, M. Dijkstra, *Nat. Mater.* **2015**, *14*, 56; g) J. W. Wang, C. F. Mbah, T. Przybilla, B. A. Zubiri, E. Spiecker, M. Engel, N. Vogel, *Nat. Commun.* **2018**, *9*, 5259; h) J. Wang, C. F. Mbah, T. Przybilla, S. Englisch, E. Spiecker, M. Engel, N. Vogel, *ACS Nano* **2019**, *13*, 9005; i) S. Park, H. Hwang, M. Kim, J. H. Moon, S. H. Kim, *Nanoscale* **2020**, *12*, 18576–18594; j) J. Lacava, P. Born, T. Kraus, *Nano Lett.* **2012**, *12*, 3279; k) V. N. Manoharan, M. T. Elsesser, D. J. Pine, *Science* **2003**, *301*, 483.

[3] a) N. Vogel, S. Utech, G. T. England, T. Shirman, K. R. Phillips, N. Koay, I. B. Burgess, M. Kolle, D. A. Weitz, J. Aizenberg, *Proc. Natl. Acad. Sci. USA* **2015**, *112*, 10845; b) E. S. A. Goerlitzer, R. N. K. Taylor, N. Vogel, *Adv. Mater.* **2018**, *30*, 1706654; c) Y. J. Zhao, L. Shang, Y. Cheng, Z. Z. Gu, *Acc. Chem. Res.* **2014**, *47*, 3632; d) P. M. Parker, G. Guidetti, C. A. Williams, T. Zhao, A. Narkevicius, S. Vignolini, B. Frka-Petesic, *Adv. Mater.* **2018**, *30*, 1704477; e) Y. Takeoka, S. Yoshioka, A. Takano, S. Arai, K. Nueangnoraj, H. Nishihara, M. Teshima, Y. Ohtsuka, T. Seki, *Angew. Chem. Int. Ed.* **2013**, *52*, 7261; *Angew. Chem.* **2013**, *125*, 7402.

[4] a) J. Wang, U. Sultan, E. S. A. Goerlitzer, C. F. Mbah, M. Engel, N. Vogel, *Adv. Funct. Mater.* **2020**, *30*, 1907730; b) M. Xiao, Z. Y. Hu, Z. Wang, Y. W. Li, A. D. z Tormo, N. L. Thomas, B. X. Wang, N. C. Gianneschi, M. D. Shawkey, A. Dhinojwala, *Sci. Adv.* **2017**, *3*, 170115; c) T. H. Zhao, G. Jacucci, X. Chen, D.-P. Song, S. Vignolini, R. M. Parker, *Adv. Mater.* **2020**, *32*, 2002681; d) T. Iwasaki, Y. Tamai, M. Yamamoto, T. Taniguchi, K. Kishikawa, M. Kohri, *Langmuir* **2018**, *34*, 11814; e) S. M. Klein, V. N. Manoharan, D. J. Pine, F. F. Lange, *Langmuir* **2005**, *21*, 6669; f) S. H. Kim, S. Y. Lee, G. R. Yi, D. J. Pine, S. M. Yang, *J. Am. Chem. Soc.* **2006**, *128*, 10897.

[5] a) P. F. Damasceno, M. Engel, S. C. Glotzer, *Science* **2012**, *337*, 453; b) E. G. Teich, G. van Anders, D. Klotsa, J. Dshemuchadse, S. C. Glotzer, *Proc. Natl. Acad. Sci. USA* **2016**, *113*, E669; c) C. X. Du, G. van Anders, R. S. Newman, S. C. Glotzer, *Proc. Natl. Acad. Sci. USA* **2017**, *114*, E3892–E3899; d) C. X. Du, G. van Anders, J. Dshemuchadse, P. M. Dodd, S. C. Glotzer, *Mol. Simul.* **2020**, *46*, 1037; e) R. K. Cersonsky, J. Dshemuchadse, J. Antonaglia, G. van Anders, S. C. Glotzer, *Phys. Rev. Mater.* **2018**, *2*, 125201; f) Y. Lu, Y. Yin, Y. Xia, *Adv. Mater.* **2001**, *13*, 415; g) R. K. Cersonsky, J. Antonaglia, B. D. Dice, S. C. Glotzer, *Nat. Commun.* **2021**, *12*, 2543.

[6] a) D. Wang, M. Hermes, R. Kotni, Y. T. Wu, N. Tasios, Y. Liu, B. de Nijs, E. B. vander Wee, C. B. Murray, M. Dijkstra, A. van Blaaderen, *Nat. Commun.* **2018**, *9*, 2228; b) J. Henzie, M. Gruenwald, A. Widmer-Cooper, P. L. Geissler, P. Yang, *Nat. Mater.* **2012**, *11*, 131–137; c) T. Wang, J. Zhuang, J. Lynch, O. Chen, Z. Wang, X. Wang, D. LaMontagne, H. Wu, Z. Wang, Y. C. Cao, *Science* **2012**, *338*, 358; d) J. M. Meijer, L. Rossi, *Soft Matter* **2021**, *17*, 2354.

[7] a) O. Yaghi, H. Li, *J. Am. Chem. Soc.* **1995**, *117*, 10401; b) H.-C. Zhou, S. Kitagawa, *Chem. Soc. Rev.* **2014**, *43*, 5415; c) H.-C. Zhou, J. R. Long, O. M. Yaghi, *Chem. Rev.* **2012**, *112*, 673; d) J. R. Long, O. M. Yaghi, *Chem. Soc. Rev.* **2009**, *38*, 1213.

[8] a) J. Cravillon, C. A. Schröder, R. Nayuk, J. Gummel, K. Huber, M. Wiebcke, *Angew. Chem. Int. Ed.* **2011**, *50*, 8067; *Angew. Chem.* **2011**, *123*, 8217; b) S. Wang, S. S. Park, C. T. Buru, H. Lin, P.-C. Chen, E. W. Roth, O. K. Farha, C. A. Mirkin, *Nat. Commun.* **2020**, *11*, 2495; c) J. Troyano, A. Carné-Sánchez, C. Avci, I. Imaz, D. Maspoch, *Chem. Soc. Rev.* **2019**, *48*, 5534; d) M. Pang, A. J. Cairns, Y. Liu, Y. Belmabkhout, H. C. Zeng, M. Eddaoudi, *J. Am. Chem. Soc.* **2013**, *135*, 10234.

[9] C. Avci, I. Imaz, A. Carné-Sánchez, J. A. Pariente, N. Tasios, J. Pérez-Carvajal, M. I. Alonso, A. Blanco, M. Dijkstra, C. López, D. Maspoch, *Nat. Chem.* **2018**, *10*, 78.

[10] C. Avci, Y. Liu, J. A. Pariente, A. Blanco, C. Lopez, I. Imaz, D. Maspoch, *Small* **2019**, *15*, 1902520.

[11] a) K. S. Park, Z. Ni, A. P. Côté, J. Y. Choi, R. Huang, F. J. Uribe-Romo, H. K. Chae, M. O'Keeffe, O. M. Yaghi, *Proc. Natl. Acad. Sci. USA* **2006**, *103*, 10186; b) X.-C. Huang, Y.-Y. Lin, J.-P. Zhang, X.-M. Chen, *Angew. Chem. Int. Ed.* **2006**, *45*, 1557; *Angew. Chem.* **2006**, *118*, 1587.

[12] J. Hafizovic Cavka, S. Jakobsen, U. Olsbye, N. Guillou, C. Lamberti, S. Bordiga, K. P. Lillerud, *J. Am. Chem. Soc.* **2008**, *130*, 13850.

[13] G. van Anders, D. Klotsa, N. K. Ahmed, M. Engel, S. C. Glotzer, *Proc. Natl. Acad. Sci. USA* **2014**, *111*, E4812.

[14] R. E. Guerra, C. P. Kelleher, A. D. Hollingsworth, P. M. Chaikin, *Nature* **2018**, *554*, 346.

[15] G. Meng, J. Paulose, D. R. Nelson, V. N. Manoharan, *Science* **2014**, *343*, 634.

[16] M. Rosenberg, F. Dekker, J. G. Donaldson, A. P. Philipse, S. S. Kantorovich, *Soft Matter* **2020**, *16*, 4451.

[17] a) G. van Anders, N. K. Ahmed, R. Smith, M. Engel, S. C. Glotzer, *ACS Nano* **2014**, *8*, 931–940; b) P. F. Damasceno, M. Engel, S. Glotzer, *ACS Nano* **2012**, *6*, 609–614.

© 2022 The Authors. Angewandte Chemie published by Wiley-VCH GmbH

15213757, 2022, 16, Downloaded from https://onlinelibrary.wiley.com/doi/10.1002/ange.202117455 by Readcube (Labtiva Inc.), Wiley Online Library on [27/10/2022]. See the Terms and Conditions (https://onlinelibrary.wiley.com/terms-and-conditions) on Wiley Online Library for rules of use; OA articles are governed by the applicable Creative Commons License

[18] R. M.Parker, T. H. Zhao, B. Frka-Petesic, S. Vignolini, *arXiv preprint* arXiv:2110.00410, **2021**.
[19] R. Ohnuki, S. Isoda, M. Sakai, Y. Takeoka, S. Yoshioka, *Adv. Opt. Mater.* **2019**, *7*, 1900227.
[20] R. Ohnuki, M. Sakai, Y. Takeoka, S. Yoshioka, *Langmuir* **2020**, *36*, 5579.
[21] a) T. Aoyagi, Y. Aoyagi, S. Namba, *Appl. Phys. Lett.* **1976**, *29*, 303; b) E. G. Loewen, M. Nevière, D. Maystre, *Appl. Opt.* **1977**, *16*, 2711; c) A. Wirgin, R. Deleuil, *J. Opt. Soc. Am.* **1969**, *59*, 1348; d) J. E. Harvey, R. N. Pfisterer, *Opt. Eng.* **2019**, *58*, 87105.

Manuscript received: December 22, 2021
Accepted manuscript online: February 7, 2022
Version of record online: February 23, 2022

© 2022 The Authors. Angewandte Chemie published by Wiley-VCH GmbH

15213757, 2022, 16, Downloaded from https://onlinelibrary.wiley.com/doi/10.1002/ange.202117455 by Readcube (Labtiva Inc.), Wiley Online Library on [27/10/2022]. See the Terms and Conditions (https://onlinelibrary.wiley.com/terms-and-conditions) on Wiley Online Library for rules of use; OA articles are governed by the applicable Creative Commons License